Eur Biophys J (2011) 40:59–68
DOI 10.1007/s00249-010-0627-6

ORIGINAL PAPER

Atomic force microscopy study of DNA conformation in the presence of drugs

Valeria Cassina · Davide Seruggia · Giovanni Luca Beretta · Domenico Salerno · Doriano Brogioli · Stefano Manzini · Franco Zunino · Francesco Mantegazza

Received: 6 July 2010 / Revised: 27 August 2010 / Accepted: 3 September 2010 / Published online: 30 September 2010

Abstract Binding of ligands to DNA gives rise to several relevant biological and biomedical effects. Here, through the use of atomic force microscopy (AFM), we studied the consequences of drug binding on the morphology of single DNA molecules. In particular, we quantitatively analyzed the effects of three different DNA-binding molecules (doxorubicin, ethidium bromide, and netropsin) that exert various pharmacologic and therapeutic effects. The results of this study show the consequences of intercalation and groove molecular binding on DNA conformation. These single-molecule measurements demonstrate morphological features that reflect the specific modes of drug–DNA interaction. This experimental approach may have implications in the design of therapeutically effective agents.

Keywords DNA · Atomic force microscopy · Doxorubicin · Ethidium bromide · Netropsin

V. Cassina (✉) · D. Seruggia · D. Salerno · D. Brogioli · F. Mantegazza
Department of Experimental Medicine,
University of Milano–Bicocca, Via Cadore 48,
20052 Monza, Milan, Italy
e-mail: valeria.cassina@unimib.it

G. L. Beretta · F. Zunino
Department of Experimental Oncology,
Fondation IRCCS Istituto Nazionale Tumori,
20133 Milan, Italy

S. Manzini
Department of Surgical Sciences,
University of Milano–Bicocca,
Via Cadore 48, 20052 Monza, Milan, Italy

Introduction

In the past decade, use of single-molecule experiments to test the effects of DNA binders on the morphology of DNA molecules has become widespread, and several examples have been reported (Walter et al. 2008; Neuman and Nagy 2008).

DNA molecular morphology is generally characterized by measuring the contour length L (which represents the length of a completely extended molecule) and the persistence length P (which measures the DNA flexibility and corresponds to the length scale over which DNA undergoes significant bending, i.e., the decay length of bending fluctuations). The most frequently used single-molecule techniques for measuring the L and P of a DNA molecule are optical tweezers (OT) (Murayama et al. 2003; Baumann et al. 1997, 2000; van Mameren et al. 2006; Moffitt et al. 2008; Noom et al. 2007), magnetic tweezers (MT) (Salerno et al. 2010; Vilfan et al. 2009; Besteman et al. 2007; Smith et al. 1992; Gosse and Croquette 2002; Strick et al. 2003), piezoelectrically controlled micropipettes (MP) (Bustamante et al. 2003), and atomic force microscopy (AFM) (Abels et al. 2005; Pope et al. 2000; Coury et al. 1996; Dame et al. 2000; MacKerell and Lee 1999; Bustamante and Rivetti, 1996; Lyubchenko et al. 1992).

Along this vein of single-molecule analysis, AFM images provide a direct tool for exploring the effects of ligands on DNA morphology. Indeed, due to its nanoscale resolution, AFM yields detailed images of DNA chains that allow the assessment of L and P (Abels et al. 2005; Pope et al. 2000; Coury et al. 1996; Dame et al. 2000).

There are several examples of AFM techniques for the study of ligand–DNA interactions. What follows is a brief description of a few relevant cases. One of the seminal works in this field was completed by Coury et al. (1996),

who analyzed AFM images to extract the binding mode, affinity, and exclusion number of DNA in the presence of different ligands [ethidium, daunomycin, and 2,5-bis(4-amidinophenyl)furan (APF)].

More recently, the cisplatin molecule, which is a well-known anticancer drug, was studied using AFM (Hou et al. 2009). By careful analysis of AFM images, DNA condensation induced by cisplatin was observed, and a model was proposed to explain the progressive globularization of DNA. With increasing concentrations of cisplatin, AFM images first showed local distortions of DNA, followed by microloops, large aggregates, and finally compact globules.

Structural changes induced by cisplatin were also studied by single-molecule force spectroscopy (Krautbauer et al. 2000). In one such example, AFM was not used for imaging; instead, it was used for exerting picoforces on single DNA molecules, which were attached between the AFM cantilever and a gold substrate. The experiments revealed significant changes in the nanomechanical properties of DNA after platination, and these changes appeared to be strongly dependent on the specific DNA sequence.

Analogously, using AFM, Mihailovic et al. (2006) measured the effect of interactions in a particular group of octahedral organometallic complexes that intercalate with DNA molecules. In the presence of different concentrations of complexes and by considering the DNA contour lengths obtained from AFM images, the interaction binding constant was derived to illustrate the difference between intercalation and groove binding.

AFM was also used to study the structural tertiary transition of plasmid DNA in the presence of ethidium bromide (Pope et al. 2000). By increasing the ethidium bromide concentration, the authors observed a progressive transition from a relaxed structure to a region of plectonemic supercoils. AFM images of DNA plasmids can directly confirm hypotheses that are suggested by other biochemical techniques such as electrophoresis (Viglasky et al. 2003). In such cases, images of DNA adsorbed onto a substrate at different temperatures and drug concentrations were acquired by AFM, which allowed researchers to distinguish the chirality assumed by the plasmid under different conditions.

Overall, these papers show that the AFM single-molecule technique can provide important descriptions of the structural aspects of DNA–ligand binding. Similarly, the general idea of the present work is to use the AFM technique to study the effects of three different ligands including doxorubicin (DOXO), ethidium bromide (ETBR), and netropsin (NETRO) on DNA molecules.

- DOXO is a well-known DNA intercalating agent, and DNA is recognized as being the primary target for its pharmacological action. Despite the central role of DNA binding in the antitumor activity of anthracyclines, available evidence indicates that the inhibition of specific DNA function is responsible for DOXO's therapeutic effects. Indeed, the primary mechanism of cytotoxic and antitumor activity by DOXO is now considered to be its interference with the function of topoisomerase II. DOXO functions as an enzyme poison by forming a DNA–drug–enzyme ternary complex, thus stabilizing the cleavable complex in which DNA strands are broken and enzyme subunits are covalently linked to DNA. Stabilization of the cleavable complex causes specific lethal DNA lesions (i.e., double-strand protein-associated DNA breaks) after interactions with enzymes involved in DNA metabolism (Minotti et al. 2004).
- ETBR is a DNA intercalating molecule without antitumor activity that is used as a laboratory tool for DNA staining (Langner et al. 2006). It has been reported that ETBR modifies the DNA contour length (Krautbauer et al. 2002; Vladescu et al. 2005; McCauley et al. 2005; Ros et al. 2004) and induces unwinding (Hayashi and Harada 2007; Wang 1974).
- NETRO is a minor groove binder that exhibits antiviral activity by inhibiting replication of DNA and RNA viruses in mammalian cells (Kopka et al. 1985). NETRO causes overtwisting of DNA chains, as shown in Triebel et al. (1994, 1995) and Snounou and Malcolm (1983).

In this work, we quantitatively analyzed AFM images of DNA in the presence of increasing concentrations of drugs, and we extracted the corresponding values of contour length and persistence length. Our quantitative analysis of AFM images yields an evaluation of the mean square values of the end-to-end distance $\langle R^2 \rangle$ versus the curvilinear coordinate s measured along the chain. Using this procedure, we can quantify the dependence of the DNA contour length L and persistence length P on the applied drug concentrations.

We detected a clear increase of L in the presence of added DOXO and ETBR, whereas the effect of NETRO on L was less obvious. All drugs induced a decrease of P. Moreover, we found that high concentrations of DOXO and ETBR caused aggregation and collapse of the DNA chains. In both cases, the aggregates appeared to be random flocks due to chain–chain interactions, but at intermediate concentrations, the DNA–ETBR data seemed to also show tertiary compact structures that resembled plectonemes. The aggregation effects were more easily induced at lower concentrations of DOXO compared with ETBR. No aggregation effects were observed with NETRO.

Materials and methods

Drug characterization

In this study, we used three different DNA binders: doxorubicin (DOXO), ethidium bromide (ETBR), and netropsin (NETRO). All three binders were purchased from Sigma Aldrich and were diluted in 0.22-μm-filtered deionized pure water.

DNA preparation for AFM measurements

For AFM studies, pUC19 plasmid DNA ($N_{bp} = 2{,}686$ bp) was used. Plasmid DNA was isolated with a QIAGEN MIDI kit and then linearized with *Eco*RI (New England Biolabs), fractionated on 1.4% agarose gel, and purified with a QIAGEN MinElute gel extraction kit with elution in 10 mM Tris-Cl, pH 8.5. To reduce spurious cuts or star activity of the restriction enzyme, no more than 5 units of *Eco*RI (New England Biolabs) were used to linearize 1 μg plasmid DNA for a cleavage time no longer than 2 h. This procedure minimized the amount of spurious fragments (see histogram in Fig. 1c). The DNA concentration used in these studies ($[DNA]_0 = 0.14$ nM) was estimated to provide reasonable DNA molecule statistics and to provide single-filament deposition on mica without superposition.

There are several strategies for DNA deposition on mica surfaces (Lyubchenko et al. 1992; Lyubchenko and Shlyakhtenko 1997; Podestá et al. 2005; Hansma et al. 1997). Here, we mainly followed the protocols of Hou et al. (2009), Lysetska et al. (2002), and Hansma and Laney (1996), in which a nickel buffer was used because it seemed to provide the strongest DNA adhesion to the mica surface.

The DNA was diluted to final concentration of 0.24 ng/μl in 2 mM Ni^{2+} and 10 mM *N*-2-hydroxyethylpiperazine-*N*′-2-ethanesulfonic acid (HEPES) at different concentrations of drug. To study the modifications of DNA morphology by AFM imaging, a 35 μl DNA solution at different drug concentrations was incubated on freshly cleaved mica (Ted Pella) at room temperature for 5 min to allow the DNA to adsorb to the surface. The sample was rinsed with 0.22-μm-filtered deionized pure water and dried with a gentle nitrogen flow.

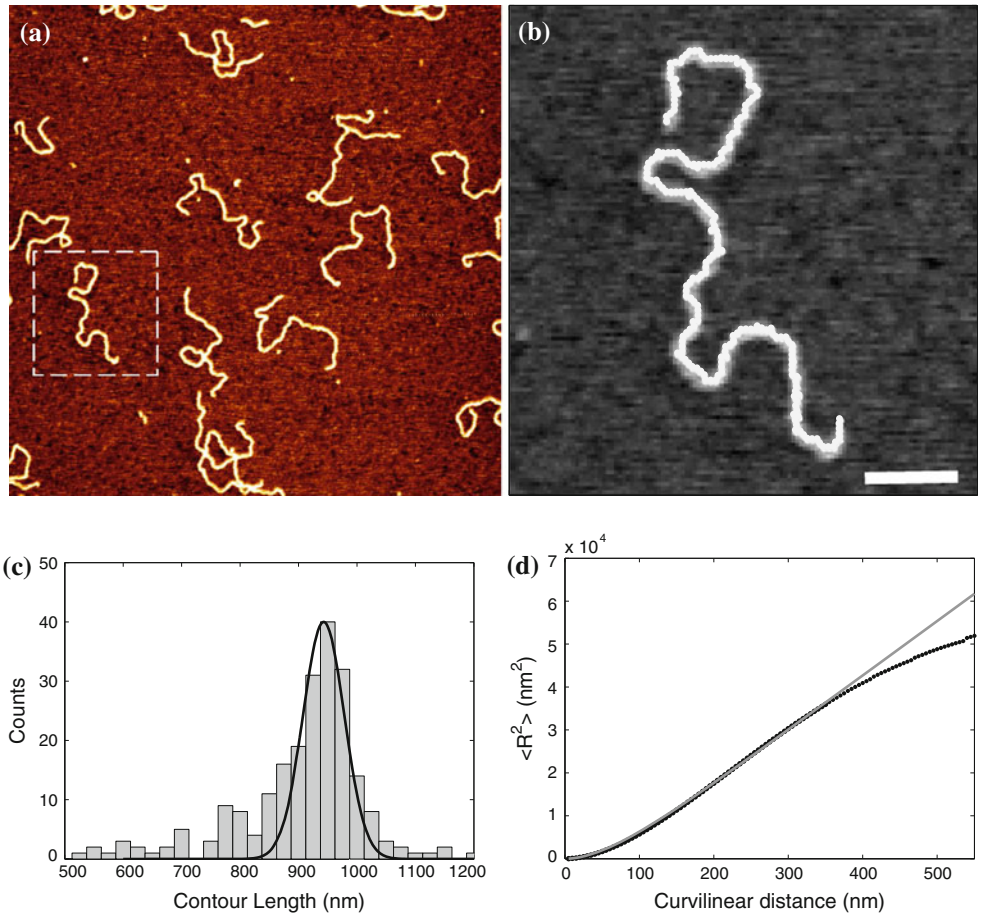

Fig. 1 **a** Representative 2 μm × 2 μm AFM image (512 × 512 pixels, *z* range 1 nm). Data were obtained for untreated DNA molecules of 2,686 bp deposited on mica using Ni^{2+} buffer. **b** Detailed magnified image of a DNA molecule tracked by a semi-automatic Matlab routine (the *scale bar* is 100 nm, *z* range 2 nm). **c** Histogram of the contour length distribution measured from AFM images and a relative Gaussian fit. **d** *Dots*: mean square values of the end-to-end distances $\langle R^2 \rangle$ plotted as a function of the curvilinear coordinate *s*; *solid line*: best fit of $\langle R^2 \rangle(s)$ as obtained by the worm-like chain model (see Eq. 1 and text for details)

AFM technique

AFM images of single DNA molecules deposited on mica surfaces were acquired with a Nanowizard II (JPK Instruments, Berlin) instrument. Measurements were performed in tapping mode in air using stiff silicon cantilevers (RTESP-Veeco, resonant frequencies of ~300 kHz, and spring constant of ~40 N/m). AFM images (2 μm × 2μm) were acquired at 1 Hz scan rate and 512 × 512 pixel resolution. All data in this study were verified by sampling a wide range of areas over the sample surfaces.

In addition to the qualitative analysis of the AFM images, to quantitatively characterize the drug effects, we considered the contour length (L) and persistence length (P) as specific functions that describe the DNA morphology and the drug–DNA binding (Coury et al. 1996; Hansma et al. 1997; Lysetska et al. 2002; Viglasky et al. 2003; Moreno-Herrero et al. 2006; Wiggins et al. 2006).

Figure 1 shows a typical representative AFM image of bare DNA and the relevant data analysis. AFM images of single DNA molecules (Fig. 1a) were filtered by JPK software and then processed by custom Matlab (The MathWorks, Natick, MA) routines. First, using a computer-aided algorithm, we tracked the digitized image of each DNA molecule, and we obtained the coordinates of the geometric two-dimensional (2D) shape of the single filaments with 5 nm step accuracy (corresponding to the minimum step value, because a pixel is 4.9 nm in size) (Fig. 1b). Then, from the track coordinates and for each filament, we evaluated both the contour length and the mean square value of the end-to-end distance $\langle R^2 \rangle$ as functions of the curvilinear coordinate (s). The average contour length L was obtained by a Gaussian fit of the contour length histogram of each experimental set. In the example shown in Fig. 1c, from the Gaussian fit (solid line), we measured an average contour length of 943 ± 50 nm, which is in agreement with the value of 913 nm that was expected for the pUC19 plasmid.

To obtain the persistence length value P by averaging several tenths of DNA filaments, the $\langle R^2 \rangle(s)$ function was acquired for each set of experiments. Then, the resulting functions ware fitted with the following expression derived from the two-dimensional worm-like-chain (WLC) model (Rivetti et al. 1996):

$$\langle R^2 \rangle = 4Ps\left(1 - \frac{2P}{s}\left(1 - e^{-\frac{s}{2P}}\right)\right). \quad (1)$$

Since high values of s involve few statistics, the fit range of s was limited to ~0–300 nm. Typically, beyond this value, the data are noisy and systematically different from the fitting curve, as shown in Fig. 1d. We found a persistence length of 39.5 ± 5 nm for the untreated DNA molecules. The value of the persistence length of DNA filaments measured in aqueous buffer on a Ni^{2+}-treated mica surface by Hansma et al. (1997) was ~30 nm, while the value measured by Lysetska et al. (2002) was ~36 nm. Both values are in close agreement with our results. This value has to be compared with other previous results, which estimated the persistence length of undamaged DNA deposited on a surface in the presence of Mg^{2+} as ≃50 nm (Rivetti et al. 1996). It is important to note that AFM measurements of persistence length are susceptible to both the particular sample preparation and the specific analysis method used (Lysetska et al. 2002; Hansma et al. 1997). In the literature, most studies on persistence length were performed on DNA deposited with Mg^{2+} (Rivetti et al. 1996; Podestá et al. 2005). In contrast, our measurements were acquired with samples deposited with Ni^{2+} buffer to enhance the adhesion of the DNA molecules (Hansma and Laney 1996).

Results and discussion

In what follows, we present representative AFM images of DNA obtained at increasing concentrations of DOXO, ETBR, and NETRO.

Figure 2 shows the data obtained in the presence of DOXO. For low DOXO concentrations, the DOXO–DNA interaction seems to have a negligible effect on the chain conformation (Fig. 2a, b), which appears unmodified in the absence of the drug (Fig. 1a). At increased DOXO concentrations, chain loops and overlaps are present with higher probability, and the filaments appear more and more aggregated and entangled (Fig. 2c). A further increase of the DOXO concentration results in the appearance of some aggregated and disordered coils (Fig. 2d) until complete DNA collapse (corresponding to 3.7 and 5.5 μM) (Fig. 2e,f).

Similarly, selected AFM images acquired in the presence of ETBR ranging from 0.18 to 50 μM are shown in Fig. 3. At low ETBR concentrations, most filaments appeared to be relaxed, with natural conformations (Fig. 3a, b), whereas aggregates and plectonemic structure were detected at higher concentrations, (Fig. 3c–e). This characteristic alteration of morphology (plectonemes) can be observed on careful inspection of the ETBR–AFM images (as shown in the enlargements of Fig. 3c, d), where the DNA appears as an interrupted fork instead of a single filament. As the ETBR concentration was further increased, the molecules were completely tangled (Fig. 3f), which resulted in a distribution of aggregated and disordered chains. Apparently, as a consequence of the presence of DOXO and ETBR, the DNA became sticky and gluey; at intermediate drug concentrations, the DNA filaments formed contacts that remain joined and form loops, whereas at high concentrations, they constituted disordered

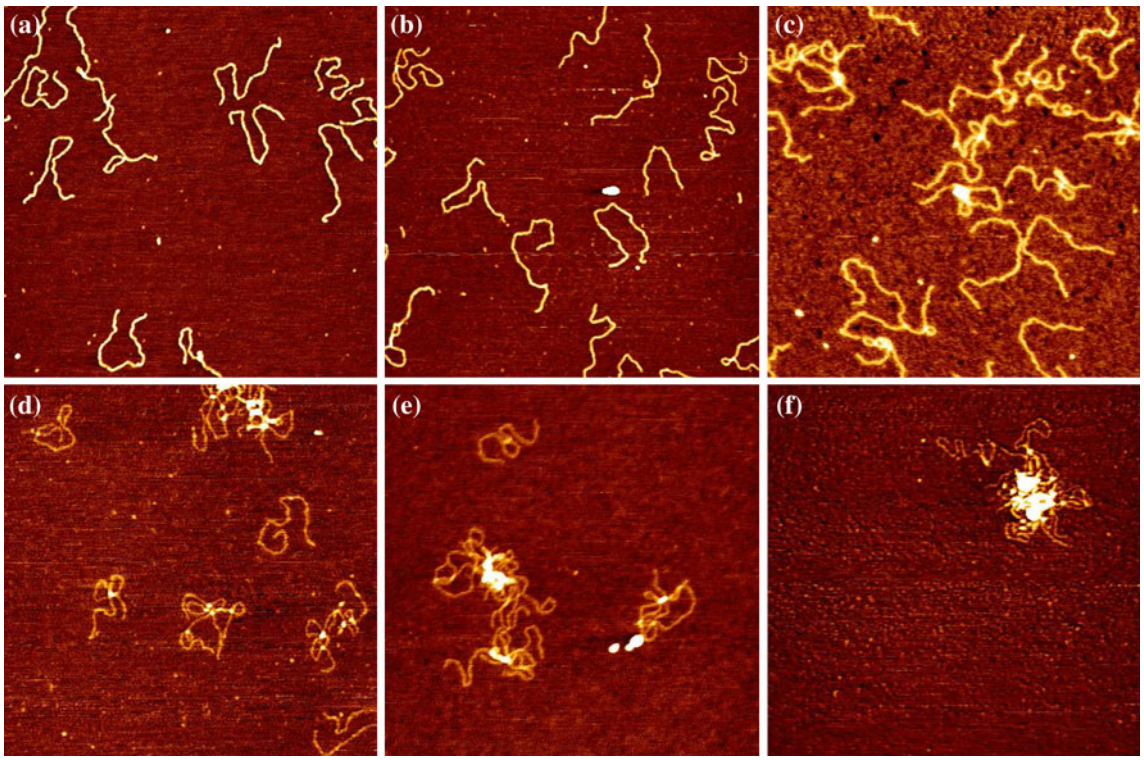

Fig. 2 AFM images of DNA (2 μm × 2 μm, *z* range 1 nm) deposited on mica in 2 mM nickel and 10 mM HEPES at different doxorubicin concentrations: **a** 0.1 μM, **b** 0.4 μM, **c** 0.7 μM, **d** 2.7 μM, **e** 3.7 μM, and **f** 5.5 μM

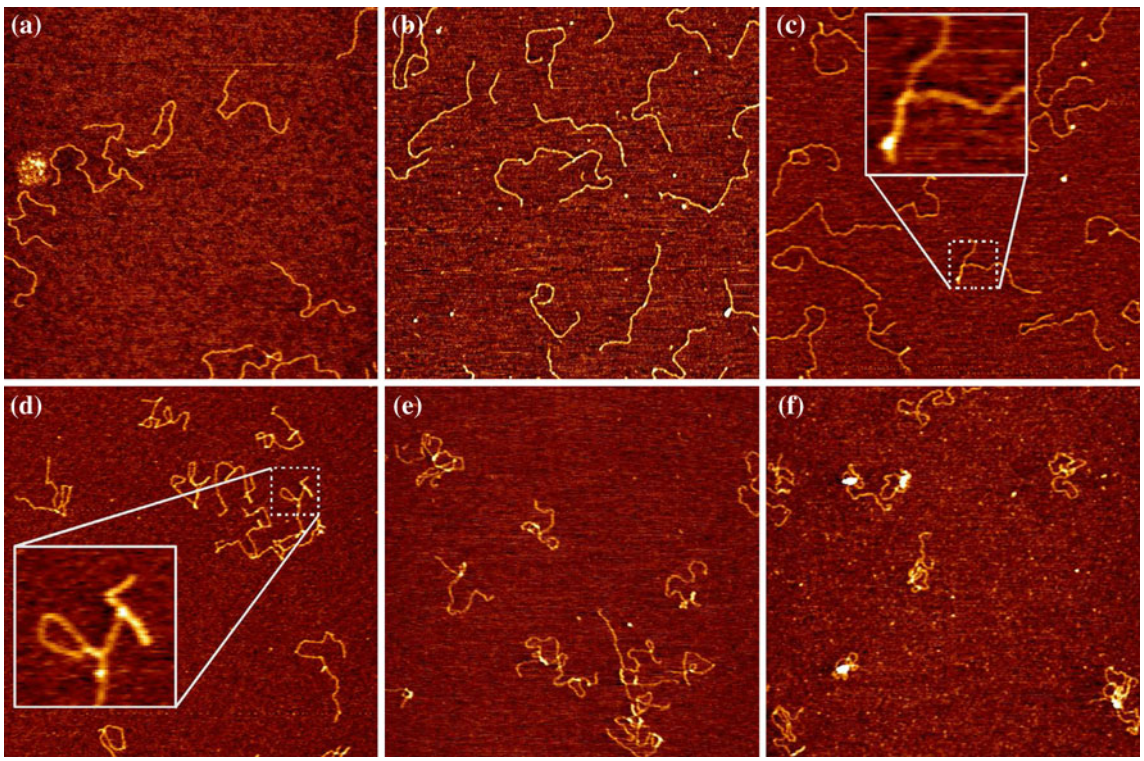

Fig. 3 AFM images of DNA (2 μm × 2 μm, *z* range 1 nm) deposited on mica in 2 mM nickel and 10 mM HEPES at different ethidium bromide concentrations: **a** 0.18 μM, **b** 0.5 μM, **c** 1 μM, **d** 5 μM, **e** 10 μM, and **f** 50 μM. Panels (**d**) and (**e**) present enlargements of the DNA details, showing the "plectonemic" fork-like structures not observed with the other DNA binders under investigation

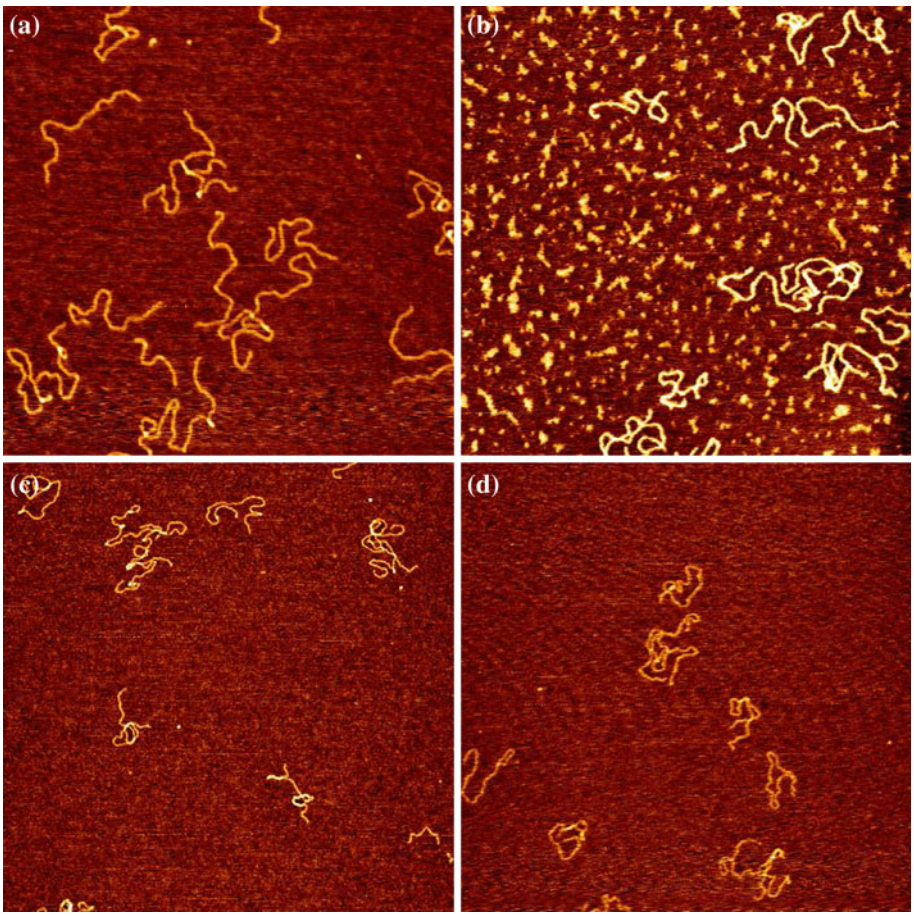

Fig. 4 AFM images of DNA (2 μm × 2 μm, z range 1 nm) deposited on mica in 2 mM nickel and 10 mM HEPES at different netropsin concentrations: **a** 0.14 μM, **b** 0.33 μM, **c** 1.4 μM, and **d** 3.3 μM

aggregates. These aggregation phenomena occurred at higher concentrations for ETBR (50 μM) than for DOXO (5.5 μM).

At comparable concentrations of drug, DNA–NETRO images (Fig. 4) did not show the above-described effects; at increasing concentrations of NETRO, no aggregation was detected despite the observed stiffness decrease. In the presence of NETRO, the average size of the DNA coils seems to decrease, but the single DNA chains are still distinguishable.

For a deeper understanding of drug–DNA interactions, we quantitatively characterized the DNA behavior by analyzing the AFM images. We tracked every distinguishable DNA molecule with suitable algorithms, and then calculated the contour length and the persistence length at various drug concentrations below the entanglement and aggregation concentrations.

Remarkably, in the presence of either DOXO or ETBR, we always observed a statistical distribution of aggregated and nonaggregated chains. At low drug concentrations, the number of aggregated chains was completely negligible, whereas with increased drug concentrations up to a limiting concentration, all chains appeared to be aggregated in collapsed coils. Above certain concentrations (Figs. 2f and 3f), the single DNA chains were indistinguishable within the aggregates; as a consequence, it was impossible to extract the contour length and persistence length using the tracking algorithm. Accordingly, our quantitative study was carried out for drug concentrations ranging up to the maximum concentration at which some single DNA filaments were still well defined, i.e., 5.5 μM for DOXO and 50 μM for ETBR.

In Fig. 5 we show, for the three drugs under investigation, the DNA contour length L as a function of the total drug concentrations obtained using the procedure described and discussed in section "Materials and methods." Accordingly, the histogram of the measured contour lengths was fitted with a Gaussian curve to provide the DNA average value and the width σ of the distribution, which is provided by the error bars $\pm\sigma$ of the Gaussian peak values. The data were obtained at fixed DNA concentration, corresponding to a base pair concentration of $[\mathrm{bp}]_0 = 0.37$ μM. The DNA length at zero drug concentration, corresponding to the drug-free DNA condition, was about 943 ± 50 nm, which is in good agreement with the plasmid pUC19 expected value of 913 nm.

As shown in Fig. 5, the contour length of the intercalated DNA molecules clearly increases in the presence of DOXO and ETBR, while the increase with NETRO is less

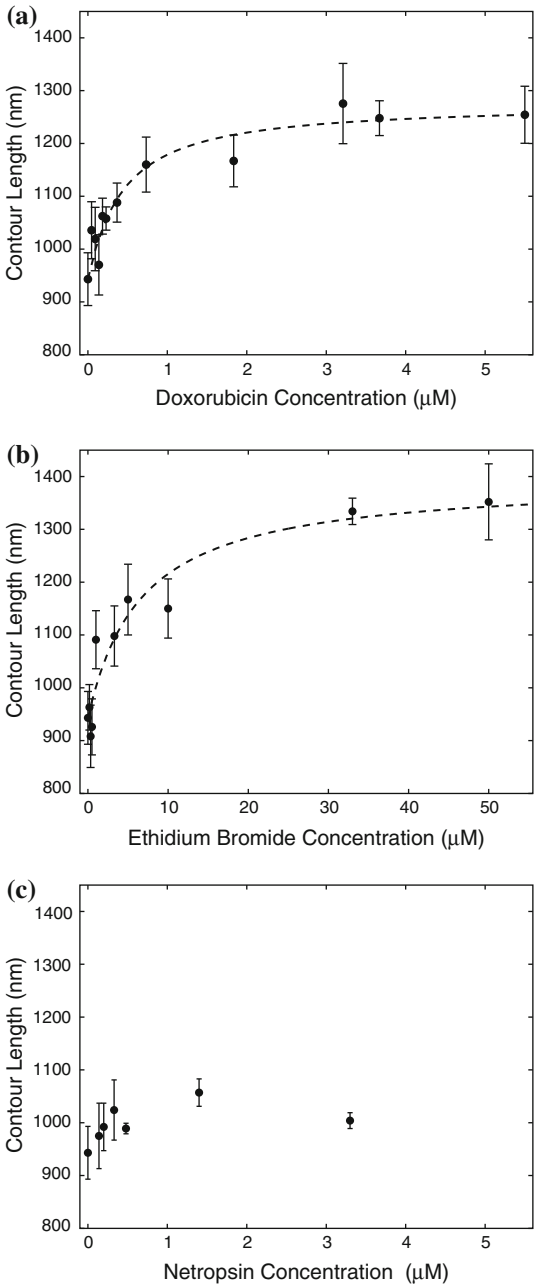

Fig. 5 DNA contour length measured as a function of the added drug concentration at fixed DNA concentrations ($[DNA]_0 = 0.14$ nM). Data obtained from analysis of AFM images (see text for details). The *dashed line* is the fitting line obtained using Eq. 5

defined. This different behavior between DOXO, ETBR, and NETRO reflects a different binding mechanism of NETRO, i.e., nonintercalating minor groove binding, which cannot be described within the same scheme of the intercalators.

At a concentration of ~ 5 μM for DOXO and ~ 35 μM for ETBR, L asymptotically reached the value of 1.25 μm for DOXO and 1.35 μm for ETBR. These values correspond to a 35% increase in length, which is similar to what was already obtained in previous comparable studies on daunomycin by Coury et al. (1996) and Rocha et al. (2007). These saturation values were attained as a consequence of the occupancy of all possible DNA intercalation sites. By assuming that each drug molecule induces a lengthening $a = 0.34$ nm for both DOXO and ETBR (Coury et al. 1996), we can estimate that DNA binding occurs about every $n \approx 3$ bp for DOXO and every $n \approx 2$ bp for ETBR [n is the so-called exclusion number (Coury et al. 1996)], where n is obtained by $n = (L - L_0)/(aN_{bp})$, L (or L_0) is the length of DNA in the presence (or absence) of drugs, and N_{bp} is the base pair number. The saturation increase in presence of NETRO is very small (of about 5%), as expected due to the minor groove binding characteristics of NETRO. Given the experimental error of the AFM measurements with NETRO, it is difficult to discriminate between a real lengthening and an effect due to the enhanced flexibility of the DNA, which results in a less accurate Gaussian fit.

By assuming the AFM-measured values of L as the reaction coordinate and by considering a classical Langmuir-like interaction between the DNA base pair (receptor) and drug (ligand), it is possible to derive a fitting equation for the DNA contour length in the presence of drug to extract the binding constant K and the exclusion number n (Lerman 1964; Pope et al. 2000). Accordingly, the interaction between DNA and drug molecules is determined by the following equations (Bornhop et al. 2007):

$$\begin{cases} K \cdot [\mathrm{bp}]/n \cdot [\mathrm{D}] = [\mathrm{B}] \\ [\mathrm{bp}]_0/n = [\mathrm{bp}]/n + [\mathrm{B}], \\ [\mathrm{D}]_0 = [\mathrm{D}] + [\mathrm{B}] \end{cases} \tag{2}$$

where $[bp]_0$ and [bp] are the molarities of the total and unbound (free) DNA base pairs, respectively, $[D]_0$ and [D] are the molarities of the total and unbound (free) drug, respectively, [B] is the molarity of the bound DNA base pairs or bound drug, and n is the exclusion number. Then, by solving the above equations, we obtain:

$$[\mathrm{B}] = \frac{K([\mathrm{bp}]_0/n + [\mathrm{D}]_0) + 1}{2K} - \frac{\sqrt{[K([\mathrm{bp}]_0/n + [\mathrm{D}]_0) + 1]^2 - 4K^2[\mathrm{bp}]_0/n[\mathrm{D}]_0}}{2K}. \tag{3}$$

Since the length of the intercalated DNA (L) is related to the length of the nonintercalated molecule (L_0) and to the single-event lengthening a, we have

$$[\mathrm{B}] = \frac{L - L_0}{a}[\mathrm{DNA}]_0 \tag{4}$$

where $[\mathrm{DNA}]_0$ is the total DNA concentration. Then, the free parameters binding constant K and binding number n can be determined by fitting the intercalated DNA contour length L (measured at concentration $[\mathrm{D}]_0$) with the following formula:

$$L = L_0 + \frac{a}{2K[\mathrm{DNA}]_0}(K(G + [\mathrm{D}]_0) + 1) - \frac{a}{2K[\mathrm{DNA}]_0}\sqrt{(K(G + [\mathrm{D}]_0) + 1)^2 - 4K^2G[\mathrm{D}]_0}, \tag{5}$$

where

$$G = \frac{[\mathrm{DNA}]_0 N_{\mathrm{bp}}}{n} \tag{6}$$

and the fixed parameters are L_0, a (estimated as 0.34 nm; Coury et al. 1996), and the number N_{bp} is the number of base pairs per DNA molecule (2,686 for pUC19).

Using the fitting procedure for DOXO and ETBR (dashed lines in Fig. 5), we obtained values of the binding affinity of $K_{\mathrm{DOXO}} = 2.6\ (\pm 0.6)\ 10^6\ \mathrm{M}^{-1}$ and of $K_{\mathrm{ETBR}} = 1.8\ (\pm 0.5)\ 10^5\ \mathrm{M}^{-1}$ and exclusion numbers of $n_{\mathrm{DOXO}} = 2.7$ and $n_{\mathrm{ETBR}} = 2$. These values should be compared with the values of $1.2\ (\pm 0.1)\ 10^5\ \mathrm{M}^{-1}$ and 2.8 obtained for the intercalator daunomycin and $6.6\ (\pm 1.9)\ 10^4\ \mathrm{M}^{-1}$ and 2 for ETBR (Coury et al. 1996; Lipfert et al. 2010; Salerno et al. 2010). Such parameters can be used as the index of binding efficiency for AFM screening of DNA interacting molecules.

To characterize the DNA in the presence of drugs, an important quantitative element is the persistence length P. Accordingly, persistence lengths of DNA filaments at different drug concentrations were calculated by fitting the measured values of the mean square value of the end-to-end distance $\langle R^2 \rangle$ as functions of the curvilinear coordinate s according to the 2D WLC model (Eq. 1).

In Fig. 6, we show the persistence length values of drug–DNA complexes as functions of the total drug concentrations for the three drugs under investigation. We observed a decrease of persistence length as a consequence of the increased DNA flexibility induced by the three drugs. The effect of ETBR on P is more relevant, since the saturation value at high drug concentrations is less than 20 nm in contrast to the value of more than 25 nm obtained with DOXO. Furthermore, for ETBR, we noted that P, which started at an initial value of about 39.5 nm, first slightly increased and then, at higher drug concentrations, decreased to a saturation value. This surprising initial increase of P as a function of the added ETBR concentration was previously observed by magnetic tweezer measurements and interpreted using an "ab initio" calculation by Rocha et al. (2007, 2009). Reflecting the different mechanics of action of NETRO with respect to DOXO and ETBR, the minor groove binder in our analysis induced a large decrease in persistence length to a value of 15 nm (Lipfert et al. 2010; Salerno et al. 2010).

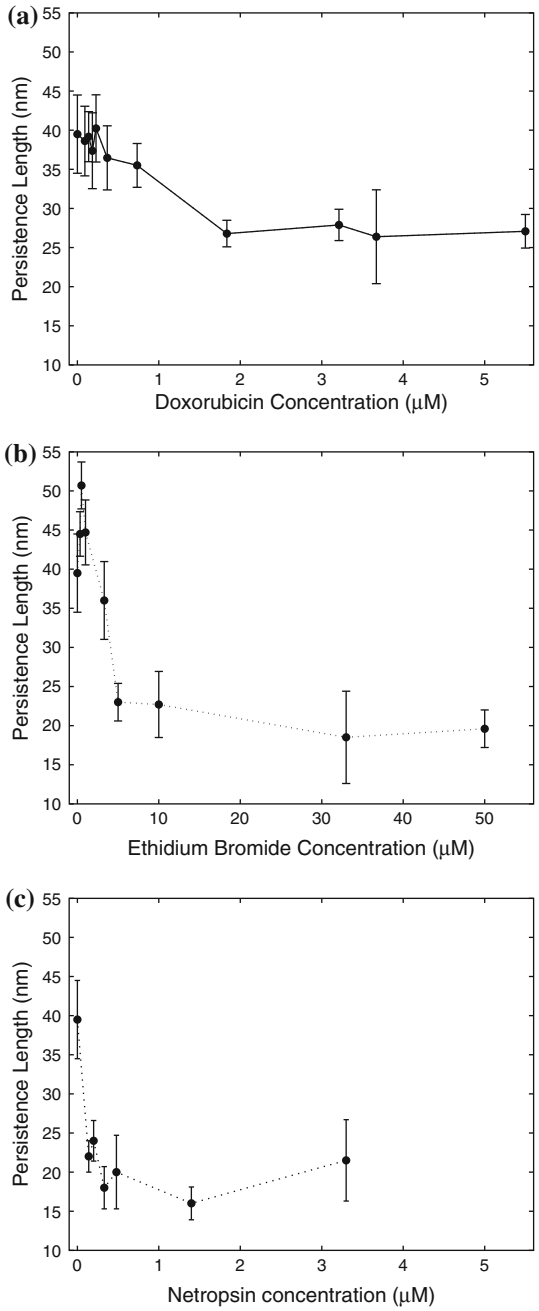

Fig. 6 DNA persistence length measured as a function of drug concentration at fixed DNA concentration ($[\mathrm{DNA}]_0 = 0.14$ nM). Data obtained from analysis of AFM images (see text for details)

Conclusions

In this work, we studied three molecules with different effects on DNA: DOXO (a DNA intercalating drug widely used for treatment of many cancers), ETBR (a mutagenic DNA intercalating agent), and NETRO (a minor groove binder possessing antiviral, antifungal, and antimicrobial properties). Using the AFM single-molecule technique, we observed the molecular effects of those binders on DNA morphology. We noticed some characteristics of the DNA–drug binding phenomenon (increasing DNA length and modified flexibility) that were not easily measurable with other standard biochemical techniques.

Furthermore, through quantitative analysis of the AFM images, we evaluated the binding constants and the exclusion numbers of the drugs under investigation. As an important outcome of this work, we observed that both the anticancer drug DOXO as well as ETBR induce a noticeable increase of the DNA contour length with respect to NETRO. In addition, the progressive aggregation of DNA molecules observed in the presence of high concentrations of DOXO and ETBR is notable. In particular, we detected aggregation of DNA molecules at lower concentrations of DOXO than those required for ETBR.

The different behavior of DOXO with respect to ETBR is likely due to different chemical features of the molecules. Indeed, the presence of an amino-sugar moiety in the DOXO structure increases the binding affinity for DNA and caused complete aggregation at low concentrations of DOXO with respect to ETBR. The complete aggregation of DNA could explain the reduced DNA damage observed in cleavage experiments performed in the presence of high concentrations of DOXO (Bigioni et al. 2001). In this regard, the production of aggregates renders the DNA less accessible by topoisomerase II and thus unavailable for the formation of a cleavable complex in this enzyme-mediated task.

Finally, based on our results, we suggest that the present approach could be a useful tool for quantitative evaluation of new molecules aimed at improving possible therapeutic effects based on their modes of DNA interaction.

Acknowledgments The authors thank D. Barisani and M. Parisotto for useful discussions and critical reading of the manuscript.

References

Abels JA, Moreno-Herrero F, van der Heijden T, Dekker C, Dekker NH (2005) Single-molecule measurements of the persistence length of double-stranded RNA. Biophys J 88:2737–2744

Baumann CG, Smith SB, Bloomfield VA, Bustamante C (1997) Ionic effects on the elasticity of single DNA molecules. Proc Natl Acad Sci USA 94:6185–6190

Baumann CG, Bloomfield VA, Smith SB, Bustamante C, Wang MD, Block SM (2000) Stretching of single collapsed DNA molecules. Biophys J 78:1965–1978

Besteman K, Hage S, Dekker NH, Lemay SG (2007) Role of tension and twist in single-molecule DNA condensation. Phys Rev Lett 98:058103/1–4

Bigioni M, Salvatore C, Bullo A, Bellarosa D, Iafrate E, Animati F, Capranico G, Goso C, Maggi CA, Pratesi G, Zunino F, Manzini S (2001) A comparative study of cellular and molecular pharmacology of doxorubicin and MEN 10755, a disaccharide analogue. Biochem Pharmacol 62:63–70

Bornhop DJ, Latham JC, Kussrow A, Markov DA, Jones RD, Sorensen HS (2007) Free-solution, label-free molecular interactions studied by back-scattering interferometry. Science 317:1732–1736

Bustamante C, Rivetti C (1996) Visualizing protein-nucleic acid interactions on a large scale with the scanning force microscope. Annu Rev Biophys Biomol Struct 25:395–429

Bustamante C, Bryant Z, Smith SB (2003) Ten years of tension: single-molecule DNA mechanics. Nature 421:423–427

Coury JE, McFaillsom L, Williams LD, Bottomley LA (1996) A novel assay for drug–DNA binding mode, affinity, and exclusion number: scanning force microscopy. Proc Natl Acad Sci USA 93:12283–12286

Dame RT, Wyman C, Goosen N (2000) H-NS mediated compaction of DNA visualised by atomic force microscopy. Nucleic Acids Res 28:3504–3510

Gosse C, Croquette V (2002) Magnetic tweezers: micromanipulation and force measurements at the molecular level. Biophys J 82:3314–3329

Hansma HG, Laney DE (1996) DNA binding to mica correlates with cationic radius: assay by Atomic Force Microscopy. Biophys J 70:1933–1939

Hansma HG, Kim KJ, Laney DE, Garcia RA, Argaman M, Allen MJ, Parsons SM (1997) Properties of biomolecules measured from atomic force microscope images: a review. J Struct Biol 119:99–108

Hayashi M, Harada Y (2007) Direct observation of the reversible unwinding of a single DNA molecule caused by the intercalation of ethidium bromide. Nucleic Acids Res 35:e125/1–7

Hou XM, Zhang XH, Wei KJ, Ji C, Dou SX, Wang WC, Li M, Wang PY (2009) Cisplatin induces loop structures and condensation of single DNA molecules. Nucleic Acids Res 37:1400–1410

Kopka ML, Yoon C, Goodsell D, Pjura P, Dickerson RE (1985) The molecular origin of DNA-drug specificity in netropsin and distamycin. Proc Natl Acad Sci USA 82:1376–1380

Krautbauer R, Clausen-Schaumann H, Gaub HE (2000) Cisplatin changes the mechanics of single DNA molecules. Angew Chem 39:3912–3915

Krautbauer R, Pope LH, Schrader TE, Allen S, Gaub HE (2002) Discriminating small molecule DNA binding modes by single molecule force spectroscoy. FEBS Lett 510:154–158

Langner KM, Kedzierski P, Sokalski WA, Leszczynski J (2006) Physical nature of ethidium and proflavine interactions with nucleic acid bases in the intercalation plane. J Phys Chem B 110:9720–9727

Lerman LS (1964) Acridine mutagens and DNA structure. J Cell Comp Physiol 64:1–191

Lipfert J, Klijnhout S, Dekker NH (2010) Torsional sensing of small-molecule binding using magnetic tweezers. Nucleic Acids Res (in press)

Lysetska M, Knoll A, Boehringer D, Hey T, Krauss G, Krausch G (2002) UV light-damaged DNA and its interaction with human replication protein a: an atomic force microscopy study. Nucleic Acids Res 30:2686–2691

Lyubchenko Y, Shlyakhtenko LS (1997) Visualization of supercoiled DNA with atomic force microscopy in situ. Proc Natl Acad Sci USA 94:496–501

Lyubchenko Y, Gall AA, Shlyakhtenko LS, Harrington RE, Jacobs BL, Oden PI, Lindsay SM (1992) Atomic force microscopy imaging of double stranded DNA and RNA. J Biomol Struct Dyn 9:589–606

MacKerell ADJ, Lee GU (1999) Structure, force, and energy of a double-stranded DNA oligonucleotide under tensile loads. Eur Biophys J 28:415–426

McCauley M, Hardwidge PR, III LJM, Williams MC (2005) Dual binding modes for an HMG domain from human HMGB2 on DNA. Biophys J 89:353–364

Mihailovic A, Vladescu I, McCauley M, Ly E, Williams MC, Spain EM, Nunez ME (2006) Exploring the interaction of ruthenium(II) polypyridyl complexes with DNA using single-molecule techniques. Langmuir 22:4699–4709

Minotti G, Menna P, Salvatorelli E, Cairo G, Gianni L (2004) Anthracyclines: molecular advances and pharmacologic developments in antitumor activity and cardiotoxicity. Pharmacol Rev 56:185–229

Moffitt JR, Chemla YR, Smith SB, Bustamante C (2008) Recent advances in optical tweezers. Annu Rev Biochem 77:205–228

Moreno-Herrero F, Seidel R, Johnson SM, Fire A, Dekker NH (2006) Structural analysis of hyperperiodic DNA from Caenorhabditis elegans. Nucleic Acids Res 34:3057–3066

Murayama Y, Sakamaki Y, Sano M (2003) Elastic response of single DNA molecules exhibits a reentrant collapsing transition. Phys Rev Lett 90:018102/1–4

Neuman KC, Nagy A (2008) Single-molecule force spectroscopy: optical tweezers, magnetic tweezers and atomic force microscopy. Nat Methods 5:491–505

Noom MC, van den Broek B, van Mameren J, Wuite GJL (2007) Visualizing single DNA-bound proteins using DNA as a scanning probe. Nat Methods 4:1031–1036

Podestá A, Indrieri M, Brogioli D, Manning GS, Milani P, Guerra R, Finzi L, Dunlap D (2005) Positively charged surfaces increase the flexibility of DNA. Biophys J 89:2558–2563

Pope LH, Davies MC, Laughton CA, Roberts CJ, Tendler SJB, Williams PM (2000) Atomic force microscopy studies of intercalation-induced changes in plasmid DNA tertiary structure. J Microsc 199:68–78

Rivetti C, Guthold M, Bustamante C (1996) Scanning force microscopy of DNA deposited onto mica: equilibration versus kinetic trapping studied by satistical polymer chain analysis. J Mol Biol 264:919–932

Rocha MS, Ferreira MC, Mesquita ON (2007) Transition on the entropic elasticity of DNA induced by intercalating molecules. J Chem Phys 127:105108/1–7

Rocha MS, Lucio AD, Alexandre SS, Nunes RW, Mesquita ON (2009) DNA-psoralen: single-molecule experiments and first principles calculations. Appl Phys Lett 95:253703

Ros A, Hellmich W, Duong T, Anselmetti D (2004) Towards single molecule analysis in PDMS microdevices: from the detection of ultra low dye concentrations to single DNA molecule studies. J Biotechnol 112:65–72

Salerno D, Brogioli D, Cassina V, Turchi D, Beretta GL, Seruggia D, Ziano R, Zunino F, Mantegazza F (2010) Magnetic tweezers measurements of the nanomechanical properties of dna in the presence of drugs. Nucleic Acids Res (in press)

Smith SB, Finzi L, Bustamante C (1992) Direct mechanical measurements of the elasticity of single DNA molecules by using magnetic beads. Science 258:1122–1126

Snounou G, Malcolm ADB (1983) Production of positively supercoiled DNA by netropsin. J Mol Biol 167:211–216

Strick TR, Dessinges MN, Charvin G, Dekker NH, Allemand JF, Bensimon D, Croquette V (2003) Stretching of macromolecules and proteins. Rep Prog Phys 66:1–45

Triebel H, Bar H, Walter A, Burckhardt G, Zimmer C (1994) Modulation of DNA supercoiling by interaction with netropsin and other minor groove binders. J Biomol Struct Dyn 11:1085–1105

Triebel H, Bär H, Geuther R, Burckhardt G (1995) Netropsin-induced changes of DNA supercoiling; sedimentation studies. Progr Colloid Polym Sci 99:45–54

van Mameren J, Modesti M, Kanaar R, Wyman C, Wuite GJ, Peterman EJ (2006) Dissecting elastic heterogeneity along DNA molecules coated partly with Rad51 using concurrent fluorescence microscopy and optical tweezers. Biophys J 91:L78–L80

Viglasky V, Valle F, Adamik J, Joab I, Podhradsky D, Dietler G (2003) Anthracycline-dependent heat-induced transition from positive to negative supercoiled DNA. Electrophoresis 24:1703–1711

Vilfan ID, Lipfert J, Kostera DA, Lemay SG, Dekker NH (2009) Magnetic tweezers for single-molecule experiments. In: Hinterdorfer P, van Oijen A (eds) Handbook of single-molecule biophysics. Springer, New York, pp 371–395

Vladescu ID, McCauley MJ, Rouzina I, Williams MC (2005) Mapping the phase diagram of single DNA molecule force-induced melting in the presence of ethidium. Phys Rev Lett 95:158102

Walter NG, Huang CY, Manzo AJ, Sobhy MA (2008) Do-it-yourself guide: how to use the modern single-molecule toolkit. Nat Methods 5:475–489

Wang J (1974) The degree of unwinding of the DNA helix by ethidium: I. titration of twisted PM2 DNA molecules in alkaline cesium chloride density gradients. J Mol Biol 89:783–801

Wiggins PA, van der Heijden T, Moreno-Herrero F, Spakowitz A, Phillips R, Widom J, Dekker C, Nelson PC (2006) High flexibility of DNA on short length scales probed by atomic force microscopy. Nat Nanotechnol 1:137–141